Antisense-Mediated Depletion Reveals Essential and Specific Functions of MicroRNAs in *Drosophila* Development

Dan Leaman,[1] Po Yu Chen,[2] John Fak,[1]
Abdullah Yalcin,[2] Michael Pearce,[1]
Ulrich Unnerstall,[1] Debora S. Marks,[3]
Chris Sander,[4] Thomas Tuschl,[2] and Ulrike Gaul[1,*]
[1]Laboratory of Developmental Neurogenetics
[2]Laboratory of RNA Molecular Biology
Rockefeller University
1230 York Ave
New York, New York 10021
[3]Department of Systems Biology
Harvard Medical School
Boston, Massachusetts 02115
[4]Computational Biology Center
Memorial Sloan Kettering Cancer Center
New York, New York 10021

Summary

MicroRNAs are small noncoding RNAs that control gene function posttranscriptionally through mRNA degradation or translational inhibition. Much has been learned about the processing and mechanism of action of microRNAs, but little is known about their biological function. Here, we demonstrate that injection of 2′O-methyl antisense oligoribonucleotides into early *Drosophila* embryos leads to specific and efficient depletion of microRNAs and thus permits systematic loss-of-function analysis in vivo. Twenty-five of the forty-six embryonically expressed micro-RNAs show readily discernible defects; pleiotropy is moderate and family members display similar yet distinct phenotypes. Processes under microRNA regulation include cellularization and patterning in the blastoderm, morphogenesis, and cell survival. The largest microRNA family in *Drosophila* (*miR-2/6/11/13/308*) is required for suppressing embryonic apoptosis; this is achieved by differential posttranscriptional repression of the proapoptotic factors *hid*, *grim*, *reaper*, and *sickle*. Our findings demonstrate that microRNAs act as specific and essential regulators in a wide range of developmental processes.

Introduction

The recent discovery of genomically encoded small RNAs, called microRNAs (miRNAs), has revealed a new mode of posttranscriptional gene regulation. miRNAs, typically 21–23 nt in length, bind to specific sequences in the 3′UTR of messenger RNAs (mRNAs), and effect mRNA degradation or inhibition of protein synthesis, depending on the degree of miRNA:mRNA complementarity (Bartel, 2004; Carrington and Ambros, 2003; Ketting and Plasterk, 2004; Lai, 2004). Biochemical and genetic efforts over the past two years have provided a great deal of insight into the underlying mechanisms, such as the synthesis and processing of miRNAs, and

the composition and function of the RNA-induced silencing complex (RISC), a ribonucleoprotein complex that incorporates the mature single-stranded miRNA and mediates the cleavage or translational repression of the target mRNA. However, our understanding of the biological function of miRNAs is still very limited, and few mRNA targets have been validated in vivo.

In plants, most mRNA targets are readily identifiable due to near-complete sequence complementarity, and miRNAs appear to act mostly by driving degradation of the target mRNA. This has greatly facilitated the functional analysis of miRNAs; in several cases, the loss of miRNA-mediated target degradation has been shown to cause severe yet specific morphological or physiological defects (Chen, 2004; Palatnik et al., 2003).

In animals, the situation is more complex. Because of the lack of strict sequence complementarity, miRNA targets in the transcriptomes of worms, flies, and humans are more difficult to detect, and miRNA-mediated regulation is likely to be more biased toward translational inhibition than mRNA degradation. Insight into the biological role of miRNAs in animals comes principally from genetics and is limited to few examples, including the control of developmental timing and cell-fate decisions in worm (Chang et al., 2004; Johnston and Hobert, 2003; Lee et al., 1993; Lin et al., 2003; Reinhart et al., 2000; Wightman et al., 1993), the control of cell growth, apoptosis and fat storage in *Drosophila* postembryonic development (Brennecke et al., 2003; Hipfner et al., 2002; Xu et al., 2003), and the regulation of insulin secretion in human (Poy et al., 2004). This paucity of functional data has precluded a comprehensive assessment of the biological relevance of miRNA-mediated gene regulation in animals.

Inspection of the experimentally validated miRNA targets and mutational analyses of known target sites suggest that strong complementarity with the 5′ end of the miRNA (positions 2–8) is critical for the recognition of target mRNAs, while pairing at the 3′ end appears to be more variable (Doench and Sharp, 2004; for review see Lai [2004]). Based on these findings, computational methods have been developed to predict miRNA targets in vertebrate and fly transcriptomes (Enright et al., 2003; Rajewsky and Socci, 2004; Rehmsmeier et al., 2004; Stark et al., 2003). Not surprisingly, the predictions are sensitive to the exact pairing rules, but all show large sets of putative targets and presumably contain both neutral and phenocritical targets (Bartel and Chen, 2004), as well as false positives. Functional information about miRNAs would help to filter the computational predictions for biologically relevant targets.

To gain broader insight into the biological role of miRNAs, we carried out a systematic analysis of miRNA function in *Drosophila* embryonic development, using an assay in which the activity of individual miRNAs is blocked in vivo by injection of antisense 2′O-methyl oligoribonucleotides and subsequent development is monitored for phenotypic abnormalities. The derivatized oligoribonucleotides are stable throughout embryogenesis and produce no unspecific defects over a

*Correspondence: gaul@mail.rockefeller.edu

wide range of concentrations. We show that antisense but not sense or scrambled 2′O-methyl oligoribonucleotides cause phenotypes and that phenotypes resulting from antisense injection are rescued by genomic overexpression of the cognate miRNAs, indicating that the observed effects are sequence specific. Using this approach, we examine all 46 miRNAs that are expressed during the first half of *Drosophila* embryogenesis, as revealed by Northern analysis. We find that more than half have internally or externally visible phenotypes, affecting a wide range of developmental processes, often very severely. We use the antisense injections in combination with genomic mutants and reporters to identify and validate the proapoptotic factors *hid*, *grim*, *reaper*, and *sickle* as phenocritical targets of the *miR-2* family. Interestingly, we find that each member of the family shows a distinct interaction profile, strongly suggesting that pairing at the 3′ end of miRNAs is biologically significant and utilized in the differential regulation of targets.

Results

2′O-Methyl Oligoribonucleotide Injection Is an Effective Method for Blocking miRNA Function

To test *Drosophila* miRNAs for function in development, we depleted individual miRNAs by injection of antisense 2′O-methyl oligoribonucleotides (2′OM-ORNs) into early embryos. 2′OM-ORNs are refractory to nucleolytic cleavage by cellular ribonucleases and therefore more stable than their ribonucleic counterparts. Antisense 2′OM-ORNs have been shown to irreversibly inhibit small RNA function in vitro and in intact cells in a sequence-specific fashion, presumably by stoichiometric binding to RISCs containing the cognate miRNA and thus preventing interaction with its mRNA targets (Hutvágner et al., 2004; Meister et al., 2004). However, it was not clear that this method would translate to the *Drosophila* embryo, and several potential problems needed to be addressed: (1) Diffusion? Due presumably to the presence of single-stranded (ss) RNA binding proteins, long (>500 nt) ss RNAs fail to diffuse in the early embryo. To test whether this might also affect the distribution of short ss RNA, we injected a fluorescently labeled 23 nt 2′OM-ORN into early embryos and found that the label disperses rapidly throughout the entire embryo (Figures 1A–1C). (2) Unspecific effects? To test whether ss 2′OM-ORNs unspecifically affect development, we injected 23 nt 2′OM-ORN antisense GFP into early embryos at a wide range of concentrations (5 μM– 2 mM), resulting in estimated end concentrations in the embryo of 0.25–100 μM (Figure 1H). No adverse effects on development were observed up to injection concentrations of 400 μM, but at 2 mM the embryos fail to differentiate and die. Interestingly, when ss oligodeoxyribonucleotides (ODNs) are injected, embryos fail to differentiate and die already at concentrations of 20 μM (Figure 1H). This indicates that embryos are in fact quite sensitive to short ss ODNs, precluding their use for miRNA depletion in vivo (Boutla et al., 2003). (3) Incorporation into RISC? Incorporation of injected ss 2′OM-ORNs into RISC could result in neomorphic effects. However, we find that antisense 2′OM-ORNs directed against GFP are unable to abrogate GFP expression in vivo, suggesting that ss 2′OM-ORNs are in fact not incorporated into RISC (Figures 1D–1G).

Several observations indicate that the phenotypic defects observed in 2′OM-ORN-injected embryos are sequence specific (for details see below): (1) 54% of the antisense 2′OM-ORNs cause specific phenotypes; 46% do not. (2) Members of the large miRNA families (*miR-2/6/11/13/308*; *miR-310/311/312/313/92*), which share the 5′ core sequence and only diverge in their 3′ portions, show similar but distinct phenotypes. (3) Antisense, but not sense or scrambled oligonucleotides, cause phenotypic defects, as shown for *miR-6, 9,* and *13.* (4) Genomic overexpression of the cognate miRNA (partially) rescues the depletion phenotype, as shown for *miR-2, 6,* and *9.*

A further measure of the efficacy of the technique is whether antisense-mediated depletion is able to phenocopy the genomic loss of function of the cognate miRNA. The only two *Drosophila* miRNAs with extant genomic knockouts are *bantam* and *mir-14*. In both cases, embryonic development is normal overall (Brennecke et al., 2003; Xu et al., 2003), a result which we reproduce by antisense 2′OM-ORN injection, although we do observe a modest increase in cell death in *bantam* depleted embryos (Figure 1I). In *bantam* genomic null larvae, imaginal disc growth is severely impaired (Brennecke et al., 2003). We find that *bantam* antisense-injected animals have markedly smaller imaginal discs in second instar (Figures 1J and 1K), indicating that miRNA depletion faithfully phenocopies the genomic loss of function and that the derivatized oligonucleotides are remarkably persistent.

Finally, we asked which portions of the antisense 2′OM-ORN are required for the depletion effect. For three miRNAs with different severe depletion phenotypes (*miR-2, 6, 31*), truncated versions of the antisense oligonucleotide were tested. In all cases, deletion of five bases complementary to either end of the miRNA (3′Δ5; 5′Δ5) mildly reduces the phenotype, but deletion of nine bases either partially (3′Δ9) or completely (5′Δ9) abolishes it (Figure 1L, coordinates relative to the miRNA). This suggests that, while annealing of the antisense 2′OM-ORN to the 5′ end of the RISC bound miRNA is essential, the 3′ end is also accessible to the injected oligonucleotides and makes a significant contribution to the phenotype. Overall, our experiments show that antisense 2′OM-ORN injection is an effective and specific technique for inhibiting miRNA function in *Drosophila* embryos.

The Screen

Since our approach is based on injection into early embryos, we focused on miRNAs with expression during the first half of embryogenesis. There are currently 78 experimentally validated miRNAs in *Drosophila* (Griffiths-Jones et al., 2003); 48 of these are unique, the remaining 30 belong to groups of identical or near-identical multiple copies or to two miRNA families (see Experimental Procedures and see Table S1 in the Supplemental Data available with this article online). For the majority of the miRNAs, the developmental expression profile had previously been established by North-
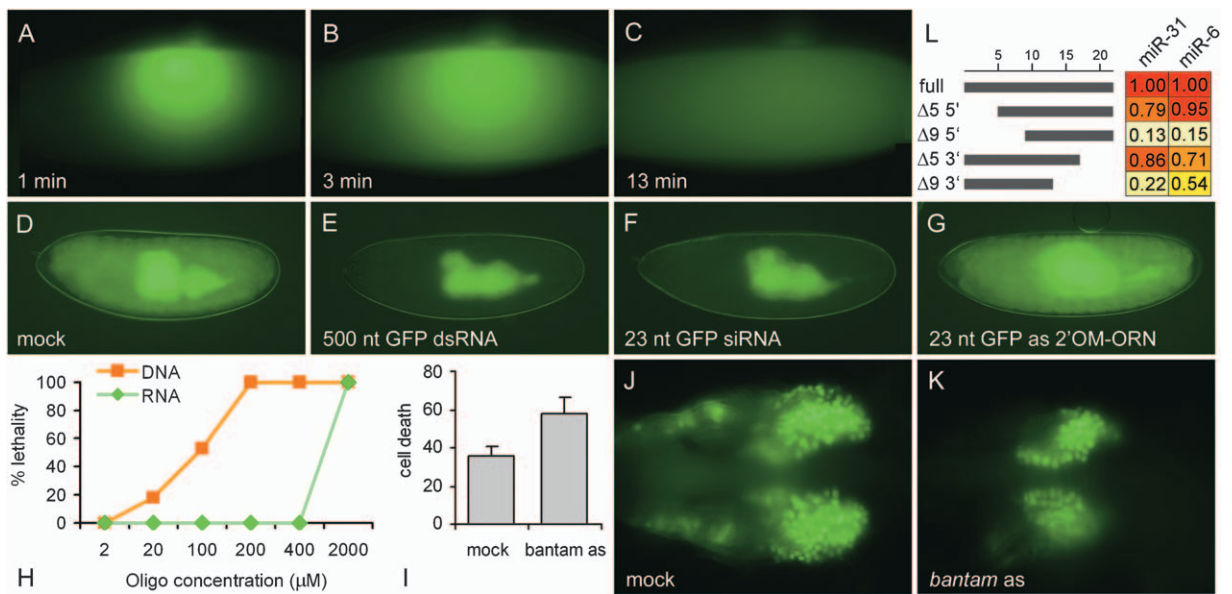
Figure 1. Establishing the Method

(A–C) Injection of fluorescein-labeled 23 nt ss 2′OM-ORN (400 μM) into young embryos (30′ AEL). The oligomer diffuses rapidly throughout the entire embryo.

(D–G) Embryos constitutively expressing nuclear GFP (*mat-Gal4;UAS-nucGFP*) (D) were injected with 500 nt GFP dsRNA (E), 23 nt GFP siRNA (F), and 23 nt antisense (as) GFP 2′OM-ORN (G). The long dsRNA and short siRNA efficiently knock down GFP expression, while the 23 nt antisense 2′OM-ORN does not, demonstrating its inability to integrate into RISC.

(H) Effects of ss ODN and ss 2′OM-ORN (GFP, *miR-7* antisense) injection on embryonic development. ss ODNs cause increasing lethality from concentrations of 20 μM upward, while ss 2′OM-ORNs show no adverse effect on development up to 400 μM.

(I–K) *bantam* antisense injection leads to a noticeable increase in embryonic cell death, as measured by the total volume of CM1-positive particles (see Experimental Procedures; columns represent mean values ±SEM; p = 0.05, t test; n = 10) (I), without affecting development or survival, but severely reduces growth of imaginal discs in second-instar larvae (48 hr) (J and K); imaginal discs are visualized live using nuclear GFP and a disc-specific driver *(ap-Gal4;UAS-nucGFP)*.

(L) Truncation analysis for *miR-31* and *miR-6*. Antisense 2′OM-ORN complementary to the indicated portion of the miRNAs were injected; based on grouping in four phenotypic classes, a score was calculated and expressed as a fraction of the score for the full-length depletion phenotype.

ern analysis (Aravin et al., 2003; Lai et al., 2003); the remainder were tested here. Of the 63 distinct miRNAs, 46 are expressed between 0 and 12 hr of embryogenesis with different temporal profiles, including uniform, maternal, early, and late zygotic (Figures S1, 4, and 5). Notably, all of the miRNAs that occur in multiple copies or belong to families are expressed during this time interval, compared to only 65% of the single-copy miRNAs.

For all 46 miRNAs showing expression in the first half of embryogenesis, 23 nt antisense 2′OM-ORNs were synthesized and purified (Experimental Procedures); for a small subset of these, sense and scrambled sequence oligonucleotides were generated to examine sequence specificity of the effect. We examined injected embryos during their development for defects using DIC to detect gross morphological abnormalities and with a live GFP marker that allowed us to gauge differentiation and morphogenesis of the nervous system (*repo-Gal4;UAS-CD8GFP*). After embryonic development was complete (24 hr), the cuticles were evaluated for defects in anteroposterior and dorsoventral pattern formation and morphogenesis. Of the 46 tested candidates, 25 showed clear morphological abnormalities, 17 visible with the live GFP marker or DIC, 25 in the

cuticle preparations. Interestingly, 87% of the multiple-copy/family miRNAs show depletion phenotypes (13 out of 15), compared to only 39% of the single-copy miRNAs (12 out of 31). In all cases, the phenotypes are highly penetrant (>50%), with several instances of clear pleiotropy. miRNAs of the same family show similar yet distinguishable phenotypes. None of the sense or scrambled 2′OM-ORNs cause phenotypic defects. The results for all tested miRNAs are collected in Table S1. A number of interesting cases with externally visible phenotypes, including the two miRNA families, were selected for further analysis and are described below.

miR-9 Affects Cellularization

Embryos injected with *miR-9* antisense 2′OM-ORNs rarely form any cuticle and show virtually no internal differentiation (Figures 2A and 2F). Examination of early embryogenesis, using phalloidin and DNA staining as well as DIC, reveal severe defects in nuclear division and migration, pole cell formation, cellularization, and in the basal movement of yolk droplets (Figures 2B–2D and 2G–2I). To establish that these defects are in fact due to depletion of *miR-9*, we tested whether they can be rescued by genomic overexpression of *mir-9*. Expression of *mir-9* with a strong maternal driver (*nos-*
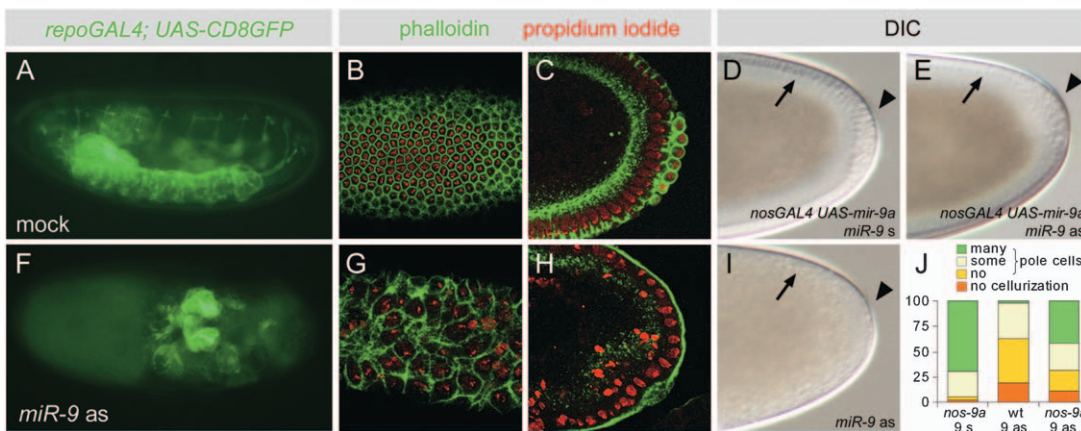
Figure 2. *miR-9* Depletion Affects Cellularization

(A and F) Differentiation assessed live in stage 16 (16 hr) embryos using autofluorescence (gut) and GFP (CNS, PNS, and salivary glands labeled by *repo-Gal4;UAS-CD8GFP*). Internal structures are fully formed in the control (A), while no differentiation has occurred in *miR-9* antisense injected embryos (F).

(B, C, G, and H) Cellularization assessed by labeling nuclei (propidium iodide; red) and actin (Alexa 488 phalloidin; green) in the blastoderm (2.5 hr); glancing view (B and G) and lateral view of the posterior (C and H). Compared to control (B and C), the actin lattice in *miR-9* depleted embryos is irregular and often encloses more than one nucleus (G); nuclei fail to form a single cortical layer, and actin ingrowth is highly irregular, with the poles being most affected (H).

(D, E, I, and J) Rescue of the *miR-9* depletion phenotype by genomic overexpression of *mir-9*. Pole cell formation (arrowheads), cellularization, and lipid droplet clearance (arrows) of injected embryos (200 μM *miR-9* sense or antisense) assessed live by DIC.

(D) Injection of *miR-9* sense (s) into embryos overexpressing *mir-9* (*nos-Gal4VP16;UAS-mir9a*) has no deleterious effect. (I) Injection of *miR-9* antisense into wild-type embryos results in a range of phenotypes, with most embryos having few or no pole cells, and some showing no somatic cellularization and lipid droplet clearance. (E) Injection of *miR-9* antisense into embryos overexpressing *mir-9* results in an amelioration of phenotypes. (J) Quantitative analysis: stacked columns show percentage of embryos with a given phenotype. p < 0.001 for the rescue experiment (*nos-Gal4VP16;UAS-mir9a*, *miR-9* antisense versus wt, *miR-9* antisense), χ^2 test, n = 40–47.

Gal4VP16;UAS-mir-9a) has no effect on its own, but significantly ameliorates the phenotype of *miR-9* antisense injection, confirming that a reduction in *miR-9* activity is responsible for the defect (Figures 2D, 2E, 2I, and 2J). Most of the processes affected by *miR-9* depletion are complex, but all share an involvement of the microtubule cytoskeleton (Lecuit and Wieschaus, 2002; Mazumdar and Mazumdar, 2002; Welte et al., 1998). Therefore, *miR-9* may have a single or a small number of phenocritical targets involved in microtubule function, but a more pleiotropic role cannot be excluded.

miR-31 Affects Segmentation

In contrast to *miR-9*, *miR-31* depleted embryos complete development but show severe segmentation defects. Embryos show abnormal cuticle patterns, ranging from partial fusions of denticle belts to a complete loss of alternating segments, suggesting that pattern formation is disrupted at the level of the pair rule genes (Figures 3A and 3E). Further examination of pair rule gene expression in the blastoderm (Carroll, 1990; Pick, 1998; Rivera-Pomar and Jackle, 1996) shows severe pattern abnormalities for *even skipped* (*eve*) and *fushi tarazu* (*ftz*), as well as *hairy* (Figures 3B–3D and 3F–3H), indicating that misregulation must occur above the pair rule gene level in the segmentation gene hierarchy. Since pattern formation is affected throughout the segmented portion of the embryo, the regional gap factors are less likely to be responsible than ubiquitous or widely expressed factors such as components of the

JAK/STAT pathway, *Dichaete*, *grainy head*, or *Grunge* (Hou et al., 1996; Nambu and Nambu, 1996; Yan et al., 1996; Zhang et al., 2002).

The *miR-310* Family Affects Dorsal Closure

Embryos injected with antisense 2′OM-ORNs for the *miR-310/311/312/313/92* family show morphogenetic defects in later development. In cuticle preparations, all family members show head-involution defects; in addition, *miR-311* and *miR-312* show mild dorsal-closure defects, and *miR-313* occasional germ band-retraction defects; *miR-310* and *miR-313* also show occasional segmentation defects (Figures 3I–3O). Germ band retraction, dorsal closure, and head involution are interconnected morphogenetic processes that share the involvement of several cellular structures and pathways, including the cytoskeleton and cell junctions, and JNK and Dpp signaling (Jacinto et al., 2002; Schock and Perrimon, 2002). Note that despite sequence identity at positions 2–8, the members of the *miR-310* family show some differences in their depletion phenotypes, suggesting that the 3′ end of the miRNA contributes to the specificity of the miRNA: mRNA pairing.

miR-2/13 and *miR-6* Depletion Results in Catastrophic Apoptosis

Embryos injected with *miR-2/13* and *miR-6* antisense 2′OM-ORNs fail to differentiate normal internal and external structures (Figures 4A, 4D, and 4G). At the end of embryogenesis, the embryos fall apart on touch, and
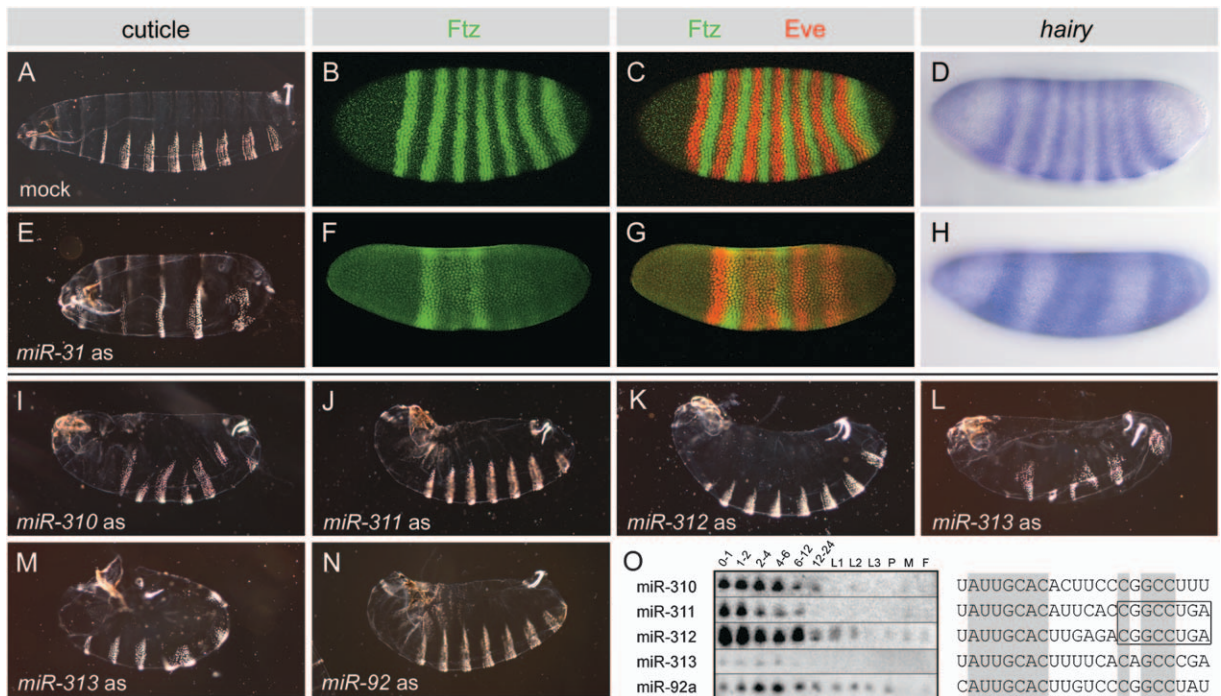
Figure 3. Effects of Depletion of *miR-31* and *miR-310* Family Members

Darkfield images of cuticle preparations (A, E, and I–N); confocal images of Eve (red) and Ftz (green) stainings (B, C, F, and G) and *hairy* RNA in situ hybridization (D and H) of blastoderm (2.5 hr) embryos.

(A–D) mock, (E–H) *miR-31* antisense-injected embryos. *miR-31* antisense-injected embryos show cuticle defects ranging from partial fusion to complete loss of segments (E), which can be traced back to abnormal pair rule gene patterning in the blastoderm. In the control (B and C), Eve and Ftz are expressed in seven largely nonoverlapping stripes, while *miR-31* antisense-injected embryos (F and G) show fewer and weaker stripes that often bleed into each other. The *hairy* transcript pattern also shows fewer stripes (H), indicating that pattern formation is affected upstream of the primary pair rule genes.

(I–N) *miR-310* family antisense-injected embryos. All family members show late morphogenetic abnormalities ranging from head involution to dorsal closure to germ band-retraction defects. In addition, some (*miR-310*, *miR-313*) show segmentation defects.

(O) Developmental Northern profiles and sequences for the members of the *miR-310* family. Identical residues are underlayed in gray.

no cuticle is recovered. To determine the onset of these problems, we examined blastoderm embryos and found that cellularization and early pattern formation along the anteroposterior axis occur normally for both miRNAs, indicating that early fating and morphogenesis are intact (Figures 4B, 4E, and 4H). Interestingly, in *miR-6*, but not *miR-2/13* depleted embryos, pole cell formation at the posterior end is disrupted (Figures 4P and 4Q).

One possible cause of the catastrophic defects observed in *miR-2/13* and *miR-6* depleted embryos is excessive and widespread apoptosis. We find that in both *miR-2/13* and *miR-6* antisense injected embryos, the number of apoptotic cells is greatly increased compared to wild-type by stage 13 (Figures 4C, 4F, and 4I). Notably, the overall morphology of *miR-6* depleted embryos is much more affected than that of *miR-2/13* depleted embryos. *miR-6* depleted embryos are generally smaller in size and have fewer and abnormally large (para-) segments, suggesting greater excess or earlier onset of apoptosis.

To determine the specificity of the effects of *miR-6* and miR-*2/13* antisense injections, we again carried out genomic rescue experiments. Embryos ubiquitously overexpressing *mir-6* or *mir-2* (*Actin-Gal4;UAS-mir6-3/2b-2*)

show normal cell-death patterns. When injected with *miR-6* or *miR-2/13* antisense, they show significant rescue of *miR-6* antisense by *mir-6*, with respect to both cell death and morphology, and of *miR-2/13* antisense by *mir-2* (see Experimental Procedures). Interestingly, crossrescue of *miR-6* antisense by *mir-2* overexpression and of *miR-2/13* antisense by *mir-6* is weak (Figures 5C, 5F, 5G, 5J, and 5K).

The miRNA sequence family *miR-6* and *miR-2/13* belong to has two additional members, *miR-11* and *miR-308*. Depletion of *miR-11* results in a moderate and of *miR-308* in a mild increase in apoptosis in midembryogenesis (Figures 4J–4O). Thus, for all members of the *miR-2* family, antisense-induced depletion results in excess embryonic cell death, but with marked differences in phenotypic strength. This differential could be due to differences in expression level or to sequence divergence and thus differential interaction with target mRNAs (Figure 4R).

The *miR-2* Family Regulates Cell Survival by Translational Repression of Proapoptotic Factors
In *Drosophila*, three pathways are known to control caspase activity (Hay, 2000; Salvesen and Abrams, 2004; Tittel and Steller, 2000). The main control is thought to
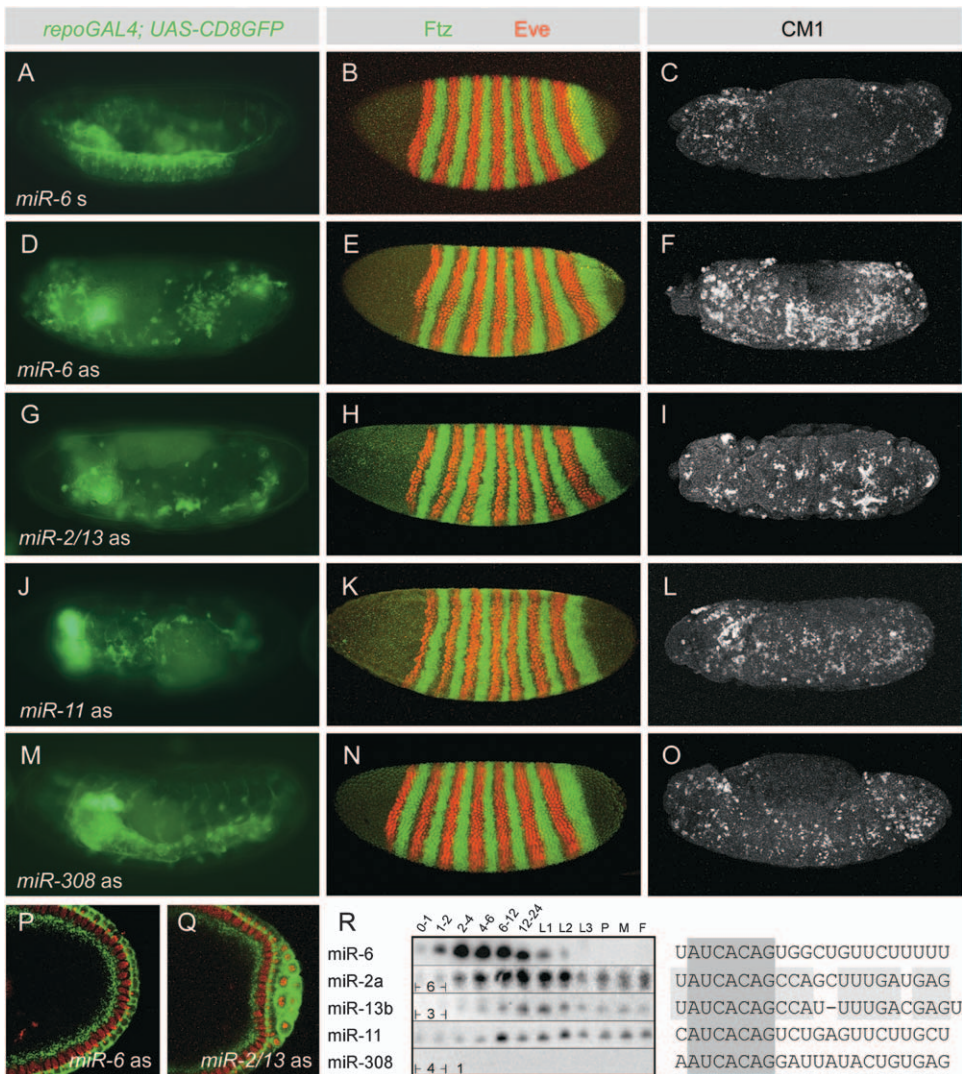
Figure 4. Depletion of *miR-2* Family Members Causes Rampant Apoptosis

(A, D, G, J, and M) Live fluorescent images of stage 16 (16 hr) embryos (*repo-Gal4;UAS-CD8GFP*); (B, E, H, K, and N) confocal images of Eve (red) and Ftz (green) stainings of blastoderm (2.5 hr) embryos; (C, F, I, L, and O) confocal images of anti-Caspase-3 (CM1) stainings of stage 13 (10 hr) embryos; (P and Q) confocal images of propidium iodide (red) and Alexa 488 phalloidin (green) stainings of blastoderm embryos. (A–C) *miR-6* sense control, (D–F and P) *miR-6*, (G–I and Q) *miR-2/13*, (J–L) *miR-11*, (M–O) *miR-308* antisense-injected embryos. In embryos depleted of *miR-2* family members, cellularization and pattern formation during blastoderm are normal (B, E, H, K, and N), yet very little differentiation is visible by the end of development (A, D, G, and J). CM1 stainings reveal severe apoptosis by midembryogenesis (C, F, I, and L). Note the following differences between family members: *miR-308* depletion causes increased apoptosis (O), but embryos complete development (M). Only *miR-6* depletion results in a loss of pole cells in ~50% of embryos (P and Q, cf. Figure 2C) and severe defects in morphological segmentation (F).

(R) Developmental Northern profiles and sequences for the *miR-2* family. Identical residues are underlayed in gray. Note that *miR-2* and *miR-13* differ in only three residues. For some family members, the number of clones recovered at early time points is indicated in the Northern profile.

come from the proapoptotic factors Hid, Grim, and Reaper (Rpr), which are transcriptionally activated in response to a range of natural and toxic conditions; they promote caspase activation through inhibition of the caspase inhibitor Diap1. The three factors appear to act independently, with each being sufficient to drive apoptosis. When *miR-2/13* and *miR-6* antisense 2′OM-ORNs are injected into embryos deficient for the *hid*, *grim*, and *rpr* genes (*H99* deficiency), they are unable

to trigger apoptosis (Figures 5B, 5E, and 5I), indicating that these miRNAs act through *hid*, *grim*, and/or *rpr*.

To determine whether the regulation of the three proapoptotic factors occurs at the transcriptional or at the posttranscriptional level, we examined their RNA expression in *miR-2/13* and *miR-6* depleted embryos using in situ hybridization and quantitative PCR. We found no significant increase in the expression level or broadening of the pattern compared to control em-
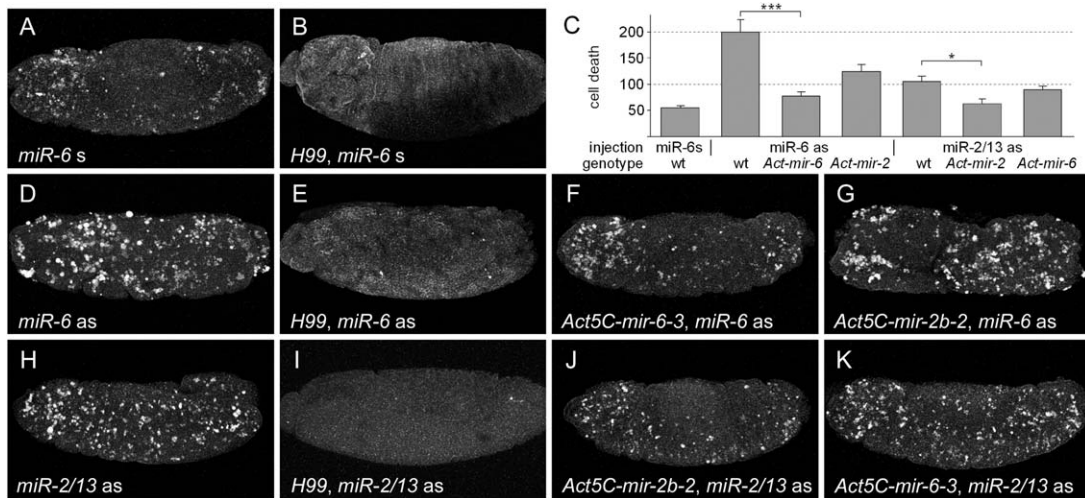
Figure 5. The Antisense-Induced Cell-Death Phenotypes of *miR-2/13* and *miR-6* Require the Presence of *hid*, *grim*, and *rpr* and Are Rescued by Genomic Overexpression of Cognate miRNA Genes

(A, B, and D–K) Projections from confocal stacks of anti-Caspase-3 (CM1)-stained embryos (stage 13 [10 hr]; lateral views); (A and B) *miR-6* sense control; (D–G) *miR-6* antisense; (H–K) *miR-2/13* antisense-injected embryos.

(A, D, and H) Wild-type; (B, E, and I) embryos homozygous mutant for the *H99* deficiency, which completely removes the *hid*, *grim*, and *rpr* genes; (F and K) embryos ubiquitously overexpressing *mir-6* (*Act5C-Gal4;UAS-mir-6-3*); (J and G) embryos ubiquitously overexpressing *mir-2* (*Act5C-Gal4;UAS-mir-2b-2*). Compared to control (A), *miR-6* antisense- (D) and *miR-2/13* antisense- (H) injected embryos show strong increase in cell death, which is completely suppressed in embryos lacking the *hid*, *grim*, and *rpr* genes (B, E, and I). Antisense-induced cell-death phenotypes are strongly rescued by genomic overexpression of the cognate miRNA gene (for *miR-6* compare [D] and [F]; for *miR-2/13* compare [H] and [J]) but less well by the other family member (compare [F] and [G], [J] and [K]). A quantification of these results is provided in (C). Cell death is measured as total volume of CM1-positive particles (see Experimental Procedures); columns represent mean values ±SEM; brackets indicate statistical significance of rescue as assessed by one-way ANOVA with Student-Newman-Keuls post hoc test: ***p < 0.001; *p < 0.05; n = 13–14.

bryos for any of three transcripts, either at embryonic stage 13 or 1 hr earlier at embryonic stage 12 (Figures 6A, 6B, 6D, 6E, 6G, and 6H and data not shown). By contrast, the protein expression of Hid (Bergmann et al., 2002) is dramatically increased in *miR-6* depleted embryos and modestly in *miR-2/13* depleted embryos (Figures 6C, 6F, and 6I). These results strongly argue against a transcriptional and in favor of a posttranscrip-

tional regulation of the proapoptotic factors by *miR-2/13* and *miR-6*.

To test this directly, we adapted two existing translation control assays to our embryonic paradigm. In the first assay, full-length 3′UTRs are fused to a ubiquitously transcribed sensor (*tub-GFP*; Brennecke et al., 2003); transgenic embryos are injected with sense or antisense 2′OM-ORNs, and GFP fluorescence is mea-
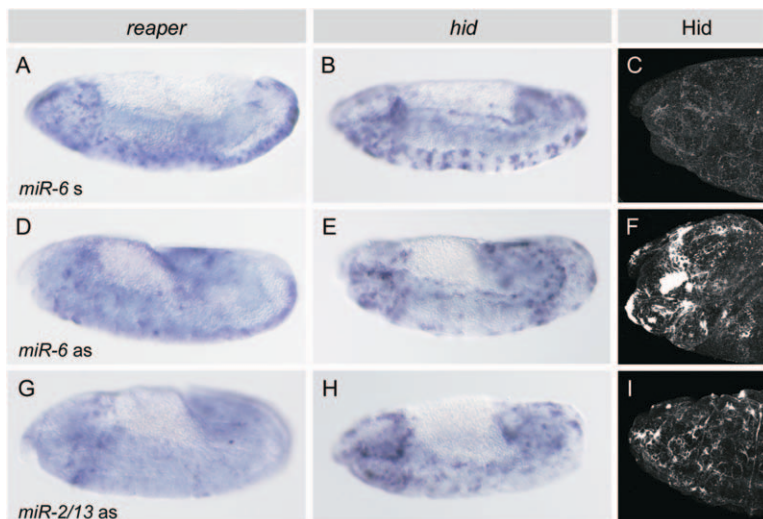

Figure 6. Effects of *miR-6* and *miR-2/13* Depletion on the Transcription and Translation of Proapoptotic Factors

(A, D, and G) *rpr* and (B, E, and H) *hid* RNA in situ hybridization of stage 13 (10 hr) embryos.

(C, F, and I) Projections from confocal stacks of Hid antibody stainings of stage 13 embryos; glancing view of the head region.

(A–C) *miR-6* sense control-, (D–F) *miR-6* antisense-, and (G–I) *miR-2/13* antisense-injected embryos. The transcript levels and patterns of *rpr* and *hid* are not significantly altered in *miR-6* and *miR-2/13* depleted embryos compared to control. In contrast, Hid protein expression levels are dramatically increased in *miR-6* depleted embryos and modestly in *miR-2/13* depleted embryos, while remaining within the wild-type domain of expression. Note that *miR-6* and *miR-2/13* depleted embryos do not complete germ band retraction.
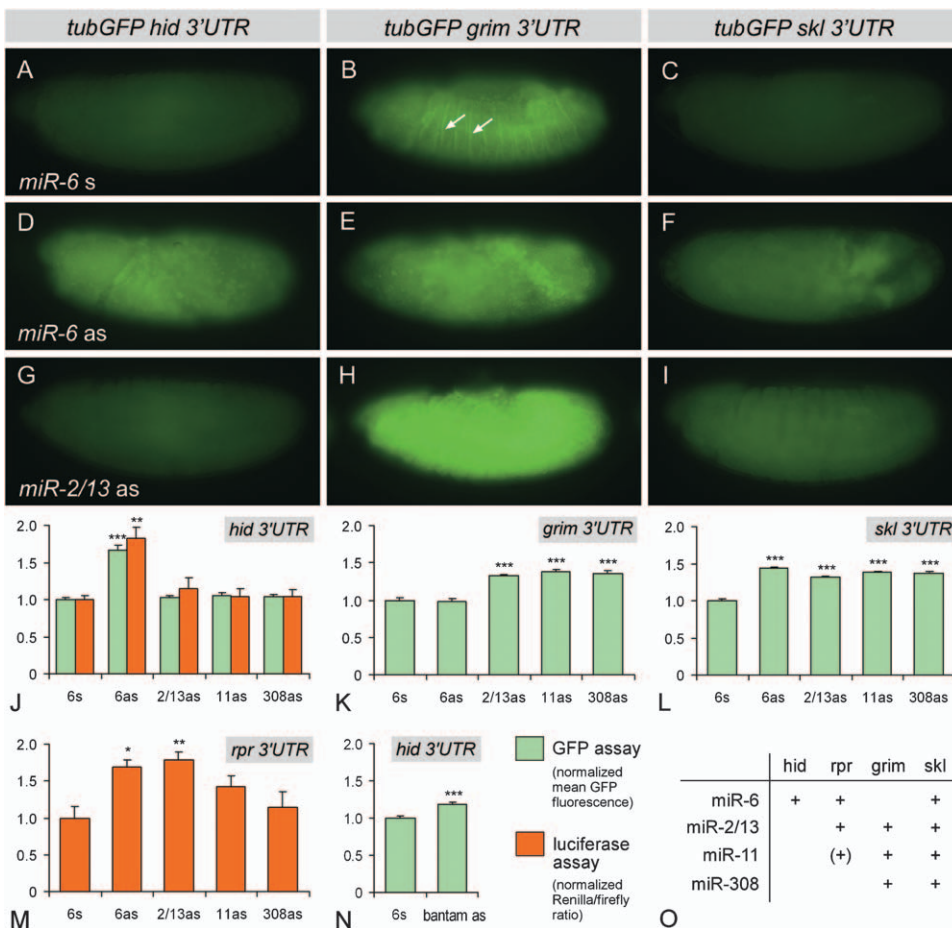
Figure 7. Effects of *miR-2* Family Depletion on the 3′ UTRs of Proapoptotic Factors

(A–I) GFP expression of stage 13 (10 hr) embryos carrying *tub-GFP-3UTR* sensors and injected with *miR-2* family sense or antisense 2′OM-ORNs; (A, D, and G) *hid*, (B, E, and H) *grim*, and (C, F, and I) *skl* GFP sensors; (A–C) *miR-6* sense-, (D–E) *miR-6* antisense-, (G–I) *miR-2/13* antisense-injected embryos in lateral view. Note the differential *grim* 3′ UTR GFP sensor expression at the segment boundaries (arrows).

(J–L and N) Quantification of all GFP sensor experiments, including for *miR-11*, *miR-308*, and *bantam* (N) antisense injections. Green columns represent mean GFP fluorescence within embryos, averaged and normalized to the value of the *miR-6* sense control (see Experimental Procedures), ± SEM, ***p < 0.001 versus *miR-6* sense; n = 18–39, t test.

(J and M) Results for transiently expressed *hid* (J) and *rpr* (M) dual luciferase sensors, coinjected with sense/antisense *miR-2* family 2′OM-ORNs into embryos. Red columns represent ratio of renilla/firefly luciferase activity, averaged over 3–5 independent replicates and normalized to the value of the *miR-6* sense control (see Experimental Procedures), ± SEM; **p < 0.01; *p < 0.05 versus *miR-6* sense, t test. In both sensor assays, the observed effects are moderate in strength but very reproducible.

(O) Summary matrix showing the statistically significant interactions between *miR-2* family members and the four proapoptotic factors.

sured live (Experimental Procedures). The 3′UTRs of *hid*, *grim*, *rpr*, and *sickle* (*skl*, a structurally related but less potent proapoptotic factor [Christich et al., 2002]) display marked differences in sensor expression, with *rpr* showing no expression, *hid* and *skl* low uniform expression, and *grim* strong and spatially modulated expression (Figures 7A–7C), indicating that these proapoptotic factors experience quite different levels of translation control. To gauge the efficacy of our assay, we injected *hid* GFP sensor embryos with *bantam* antisense 2′OM-ORNs and found mild but statistically significant derepression of GFP expression as compared to control (Figure 7N), consistent with the weak cell-death phenotype of *bantam* depleted embryos (cf. Figure 1I). Antisense injection of *miR-2* family members reveals strong derepression of the *hid* GFP sensor by

miR-6 antisense, but not by *miR-2/13*, *11*, or *308* antisense. Conversely, the *grim* GFP sensor shows significant derepression as a result of *miR-2/13*, *11*, and *308*, but not *miR-6* depletion. Finally, the *skl* GFP sensor shows significant derepression for all four family members (Figures 7A–7L).

To assess effects on *rpr*, we developed a second, more sensitive assay that employs transient expression of a dual-luciferase vector in injected embryos (Experimental Procedures). For initial comparison with the GFP assay, we tested a *hid* luciferase sensor against the entire *miR-2* family and found the same profile (Figure 7J). The *rpr* luciferase sensor shows strong derepression in *miR-6* and *2/13*, moderate derepression in *miR-11*, and no significant effect in *miR-308* depleted embryos (Figure 7M). Thus, the 3′UTRs of all four pro-

apoptotic factors are subject to translational repression by the *miR-2* family, but each miRNA displays a distinct interaction profile (Figure 7O). The interaction preferences correlate well with the observed differences in phenotype: *miR-6* has the most severe death phenotype and is the only family member to regulate *hid*, the factor with the broadest expression and the strongest proapoptotic effect. *mir-2/13* and *miR-11* have the same overall profile, but they differ in the strength of their interaction with *rpr* and show a corresponding differential in phenotypic strength. Finally, *miR-308*, which has the mildest death phenotype, interacts only with the weakly proapoptotic *skl* and with *grim*.

The differences in target interaction profile between the *miR-2* family members are pronounced and do not merely reproduce differences in the strength or onset of miRNA expression (cf. Figure 4R). This suggests that differential pairing outside the 5′ core sequence shared by all members has an important role in target selection. Computational predictions indicate that *miR-2* family binding sites are present in the 3′UTRs of all four proapoptotic factors: *rpr* and *grim* have one, *hid* and *skl* two predicted sites (Enright et al., 2003; Stark et al., 2003). All six miRNA target sites lie in sequence blocks that are conserved between the six sequenced Drosophilid species, spanning an evolutionary distance of 40 Myr (for all alignments see Figure S2). Interestingly, for all sites, absolute conservation extends well beyond the bases complementary to the 5′ core of the miRNA and includes adjacent stretches suitable for pairing with the 3′ end. All but one of the sites show Watson-Crick pairing with miRNA positions 2-7 and variable pairing at the 3′ end. One of the *hid* sites (*hid468*) has a mismatch in the core but shows strong pairing with *miR-6* at the 3′ end. The rules for 3′ pairing between miRNAs and their targets are not yet well understood, but it is clear that the *miR-2* family members differ considerably in their ability to form 3′ matches with the six target sites (Figure S2). Further experimentation will be required to better understand how the observed differences in regulatory effect relate to differences in sequence pairing.

Discussion

Using antisense 2′OM-ORN-mediated depletion, we have examined the function of all miRNAs that are expressed in early *Drosophila* embryonic development. The approach was adapted from biochemical studies that had successfully employed the method in vitro and phenocopied *let-7* genomic mutants in *C. elegans* (Hutvágner et al., 2004; Meister et al., 2004). The desired reaction of the injected antisense ORN is hybridization to the RISC bound endogenous miRNA, thus rendering it nonfunctional. Our control experiments indicate that the technique is effective and specific in blocking miRNA function. We did not observe unspecific effects on development through a wide range of injection concentrations. Our finding that the phenotypes induced by antisense 2′OM-ORN injection are cleanly rescued by genomic overexpression of the cognate miRNA gene suggests that hybridization of the antisense ORNs to mRNAs resulting in "off-target"

RNAi or translational regulation is not a significant problem.

A major focus of current miRNA research is the identification of mRNA targets. This effort has relied mainly on the use of sensor constructs and, in fly, on overexpression, leaving the question of the biological role of miRNA-mediated regulation largely unaddressed. Here, we have described a method that permits systematic loss-of-function analysis of miRNAs in vivo and on a large scale. As we demonstrate, the technique can be used not only for genome-wide phenotypic screening, but also for a detailed subsequent characterization of phenotypes using markers and epistasis experiments, thereby placing miRNAs more precisely within biological processes and pathways. Genes participating in these processes can then be scanned for the presence of miRNA binding sites to identify mRNA target candidates and narrow down the often extensive lists of computational target predictions (Enright et al., 2003; Lai, 2004; Stark et al., 2003). Finally, antisense-mediated depletion can be employed in combination with luciferase and GFP sensor constructs to directly test candidate 3′UTRs. The method thus provides a means of connecting miRNA target identification with biological function and of distinguishing phenocritical from neutral targets. We expect this approach to be effective not only in the more detailed investigation of the phenotypes reported here, but also in studying miRNA function in other developmental contexts and organisms.

The obvious alternative to inhibiting miRNA function by antisense injection is to generate genomic mutants. However, reverse genetic analysis on a large scale is laborious and particularly challenging in the case of many miRNAs, due to redundancy and complex genomic organization (e.g., clustering of unrelated miRNAs, dispersal of multicopy miRNAs among different regions of the genome; see Aravin et al., 2003, Lai et al., 2003, and Table S1). A potential limitation of a hybridization-based approach is crossreactivity. We generally expect crosshybridization of antisense ORNs to miRNAs with very close sequence similarity, i.e in the case of multicopy groups. However, these miRNAs are likely to have very similar target interactions and may in fact have to be removed as a group—either genomically or by antisense injection—to reveal their function. We find that the antisense injection approach is sufficiently specific to distinguish between more distantly related miRNAs, as in the case of miRNA families: family members show distinct phenotypes and target interaction profiles, as well as differential rescue ability. Overall, while the generation of genomic knockouts remains desirable for an in-depth study of individual miRNAs, we believe that antisense-mediated depletion will provide a powerful complementary tool for the investigation of miRNA function.

Our screen affords an assessment of the biological role of miRNAs on a larger scale. Upon depletion, 54% of the miRNAs that are expressed during the first half of *Drosophila* embryogenesis display readily discernible, often severe phenotypic defects. While displaying some pleiotropy, the miRNA depletion phenotypes are clearly distinct from one another and readily fall into different groups and categories previously identified in (forward) genetic screens. This result has several impli-

cations: it shows that miRNA-mediated regulation is essential for specific processes and that, within a given pathway, their role may be as important as that of any other negative regulator. It further suggests that individual miRNAs have a relatively small number of phenocritical targets or, perhaps more likely, multiple targets that participate in the same biological process (Bartel and Chen, 2004). Finally, the fact that the depletion of individual miRNAs can cause phenotypes implies that redundancy between distinct miRNAs is limited.

It is instructive to separately consider unique miRNAs and those that occur in multiple copies or families. Of the single-copy miRNAs, 65% are expressed in the first half of embryogenesis and 39% of those show phenotypes in our assays, while all multicopy/family miRNAs are expressed during this period and 87% show phenotypes. This suggests that, overall, the unique miRNAs have more restricted expression profiles and more specific functions, some of which may not have been captured in our assays, while the multicopy/family miRNAs show broader expression profiles and more general function. miRNA gene amplification therefore serves as a strong indicator for essential function.

We find several major developmental processes to be under miRNA control, including segmentation, cellularization, head involution/dorsal closure, and cell survival, as well as the development of the nervous system and other internal organs. Thus, our study provides strong experimental support for the notion that miRNAs represent an essential layer of gene regulation in many biological contexts. Since the discovery of miRNA genes is not complete and our screen did not exhaustively assay all aspects of development, future work will likely uncover many additional functions for miRNAs.

A particularly important task of miRNAs in *Drosophila* appears to be the regulation of cell survival. *bantam* and *mir-14* are required for suppressing apoptosis in postembryonic development (Brennecke et al., 2003; Xu et al., 2003). We have now shown that the *miR-2* family is required for suppressing apoptosis in embryogenesis. With a total of 13 copies, it is the largest miRNA family in *Drosophila*. All family members are expressed during early embryogenesis, some throughout the life cycle. Depletion of *miR-2* family members leads to increases in cell death of differing severity; the more dramatic phenotypes resemble the effect of removing the antiapoptotic factor Diap1 (Wang et al., 1999).

Several lines of evidence demonstrate that the proapoptotic factors *hid*, *grim*, *rpr*, and *skl* are phenocritical mRNA targets of the *miR-2* family. The miRNA depletion-induced cell death requires the presence of *hid, grim*, and *rpr*, indicating that derepression of downstream death effectors such as caspases is not responsible. Rampant cell death such as found in *miR-2* family depleted embryos can be triggered by developmental (mis-) cues or genotoxic stress; in these cases, transcript levels of *rpr* and *grim* are typically massively increased (Nordstrom et al., 1996). By contrast, the transcript patterns and levels of *hid*, *rpr*, and *grim* are not significantly altered in *miR-2/13* and *miR-6* depleted embryos. Hid protein levels, however, are strongly elevated in *miR-6* depleted embryos, suggesting the loss of posttranscriptional control of the proapoptotic fac-

tors as the responsible mechanism. The 3′UTRs of all four proapoptotic factors contain target sites for *miR-2* family members that are highly conserved among Drosophilids. When tested in sensor assays, the 3′UTRs of the four proapoptotic factors confer translational repression; depletion of *miR-2* family members leads to selective derepression. All four miRNAs interact with at least two of the 3′UTRs, but in different combinations. The different target interaction profiles correlate well with the differences in phenotypic strength; the data suggest that the observed phenotypes are the result of parallel action of *miR-2* family members on multiple proapoptotic factors, indicating that miRNAs can affect a biological process by targeting multiple participating mRNAs. A role for *miR-2* in regulating cell survival was first suggested by Stark et al. (2003), who showed that *mir-2b* overexpression represses *rpr*, *grim*, and *skl* GFP sensors in the wing disc but did not establish the biological significance of these interactions. Posttranscriptional control of the proapoptotic factors in general and *hid* in particular during embryonic development had been proposed early on, based on the divergence between the cell death pattern and transcript expression (Chen et al., 1996; Grether et al., 1995; White et al., 1994). Our results now identify miRNA-mediated translational repression by the *miR-2* family as a key mechanism.

All our data support the idea that miRNA:mRNA pairing at the 3′ end of the miRNA is biologically significant and utilized in the differential regulation of targets, at least for miRNA families. The truncation analysis (*miR-2, 6, 31*) suggests that the 3′ portion of endogenous RISC bound miRNAs is accessible to the injected antisense ORNs and that this interaction is necessary for generating the depletion phenotype. The differences between miRNA family members, which only diverge in their 3′ portion, in both phenotype (*miR-310* and *miR-2* families) and target interaction (*miR-2* family), suggest that there is a corresponding phenocritical interaction between the 3′ end of the miRNA and its mRNA target. The functional differences between family members and thus the importance of the 3′ end are further underscored by the finding that genomic overexpression results in strong self-rescue but weak crossrescue of the depletion phenotype (*miR-2, 6*).

An important goal of future research will be to further explore the function of miRNAs and identify their mRNA targets, as well as to determine how miRNA expression is controlled at the transcriptional level. Connecting miRNAs to both upstream and downstream events will place them firmly within the regulatory networks that govern developmental processes.

Experimental Procedures

Oligonucleotide Synthesis and Northern Analysis

ODNs were synthesized at 0.2 μmol scale using standard DNA phosphoramidite reagents (Proligo) and deprotected for 16 hr at 55°C in 1 ml of 30% aqueous ammonia. To avoid any toxicity to the embryo, the ODN was ethanol-precipitated twice from 0.3 M NaCl-containing solution and dissolved in injection buffer (20 nmol aliquots). 2′OM-ORNs were synthesized using 5′-silyl, 2′-O-methyl phosphoramidites and 0.2 μmol 3′ C6 aminolinker synthesis columns (Dharmacon Research), deprotected as described previously (Meister et al., 2004) and provided for injection as described above.

Antisense-GFP 2′OM-ORN was fluorescently labeled using a 3′ C6 aminolinker and 6-(fluorescein-5- (and 6)-carboxamido)hexanoic acid, succinimidyl ester (Molecular Probes) using standard procedures, purified by denaturing PAGE and provided for injection as described above. Northern analysis of *Drosophila* miRNAs was carried out as described in Aravin et al. (2003).

Of the 78 recorded and experimentally validated *Drosophila* miRNAs, 48 have unique sequence (Aravin et al., 2003). The remaining 30 either belong to groups of identical or near-identical copies or are members of a family; they comprise a total of 15 distinct sequences. There are two major miRNA families (*miR-310/311/312/313/92*; *miR-2/13/6/11/308*), which share the 5′ core sequence (positions 2–8) but differ in the 3′ portion; within these families, sequence divergence ranges from 5 to 14 bases out of the 22 bases total. The miRNAs in the eight known multicopy groups typically differ in 1–3 bases and are designated by letter and number suffixes (e.g., *13a*, *13b1*, *13b2*). Since we expect crosshybridization in cases of near-identical sequence, we selected one of the copies of the multicopy miRNAs for 2′OM-ORN synthesis. Members of the two families were treated separately, with the exception of *miR-2* and *miR-13*. Since they differ by only 3 bases, they were synthesized separately but the oligonucleotides were mixed for the injection. The sequences for all synthetic oligomers are collated in Table S1, including antisense, sense, mismatch, and scramble 2′OM-ORNs and ODNs.

Microinjection and Phenotypic Analysis

Embryos (*repo-Gal4;UAS-CD8GFP*) were injected with 5% egg volume 30′ AEL as previously described for RNAi (Kennerdell and Carthew, 1998), except that the point of injection was dorsal and the concentration of the 2′-OM-ORNs was 400 μM. The development of the embryos was examined live after 3 hr (blastoderm; DIC) and again after 16 hr (stage 16; GFP fluorescence). After 24 hr (end of embryogenesis), cuticles were prepared. As control, embryos were injected with buffer alone ("mock"; 0.5 mM NaPO$_4$, 5 mM KCl) or with *miR-6* sense.

RNA in situ hybridization was performed as described by Noordermeer and Kopczynski (http://www.fruitfly.org/about/methods/RNAinsitu.html), except that after staining the embryos were rinsed three times with 100% ethanol before mounting in glycerol. For immunhistochemistry, the following antibodies were used: rabbit anti-CM1 1:1000 (Cell Signaling Technology), guinea pig anti-Hid (H.-D. Ryoo), guinea pig anti-Eve 1:1000 (J. Reinitz), rabbit anti-Ftz 1:350 (H. Krause). Propidium iodide (Sigma) was used to stain nuclei at 15 μg/ml. Alexa fluor 488 phalloidin (Molecular Probes) was used at 10 units/ml. Confocal images were captured on an upright Zeiss LSM 510 confocal microscope.

CM1-positive particles often clump together; in order to accurately quantify the amount of cell death in embryos, we therefore created 3D reconstructions of confocal stacks (45 μm) and calculated isosurfaces with appropriate thresholding, using Imaris 4.0 software (Bitplane); the total volume enclosed by the isosurfaces was taken as the measure of cell death. All data were collected with identical microscope and software parameter settings. Statistical significance of differences between experiments was assessed by one-way ANOVA with Student-Newman-Keuls post hoc test, with n = 13–14.

3′UTR Sensor Assays

Embryos transgenic for ubiquitously expressed GFP sensors containing the full-length 3′UTR of *hid*, *grim*, *rpr*, and *skl* (Brennecke et al., 2003; Hipfner et al., 2002) were injected with 2′OM-ORNs as described above, and their GFP fluorescence was imaged live at 10 hr development using a Zeiss Axiophot microscope fitted with an Axiocam HR digital camera. The average pixel intensity within each embryo was measured using Metamorph 6.1 software (Universal Imaging). For each tested 3′UTR:2′OM-ORN injection combination, two to four independent injections with at least eight embryos per injection were used (n = 18–39); averages over all embryos were calculated and normalized to the average for the *miR-6* sense control. All data were collected with identical microscope, camera, and software settings. Statistical significance of differences was assessed using the t test.

For dual-luciferase reporter assays, full-length 3′UTRs of interest were cloned 3′ to Renilla luciferase; the second reporter, firefly luciferase, serves as reference (psiCHECK-2, Promega). The constructs were injected as plasmids (1 μg/μl) mixed with sense or antisense 2′OM-ORN (400 μM) into early embryos as descibed above. After 10 hr development, embryos were washed and lysed under agitation (30 animals, 60 μl lysis buffer, 30′, 750 rpm, RT). The resulting lysate was cleared by centrifugation and three aliquots were tested for luciferase activity following manufacturer's instructions. The Renilla:firefly luciferase ratios from three to five independent replicates were averaged and normalized to the value of the *miR-6* sense control. Statistical significance was assessed using the t test.

Fly Strains and Construction of miRNA Transgenes

The following strains were used: *Def(3L) H99* (H. Steller), *nos-Gal4VP16* (R. Lehmann), *repo-Gal4* (V. Auld), *Gp5V32A-Gal4*, *Actin-Gal4*, and *ap-Gal4* (Bloomington Sock Center), *UAS-CD8GFP* (L. Luo), *tub-GFP-3UTR hid/rpr/grim/skl* (S. Cohen). The genomic miRNA constructs were generated by cloning genomic PCR products comprising individual miRNA genes and flanking regions (∼1.5 kb) into the pUAST vector (Brand and Perrimon, 1993), for *mir-9a* a 1.817 kb fragment containing 0.587 kb upstream and 1.208 kb downstream, for *mir-2b2* a 1.563 kb fragment, containing 1.352 kb upstream and 0.188 kb downstream; for *mir-6-3* a 1.663 kb fragment, containing 0.091 kb upstream and 1.550 kb downstream.

Supplemental Data

Supplemental Data include two figures and one table and can be found with this article online at http://www.cell.com/cgi/content/full/121/7/1097/DC1/.

References

Aravin, A.A., Lagos-Quintana, M., Yalcin, A., Zavolan, M., Marks, D., Snyder, B., Gaasterland, T., Meyer, J., and Tuschl, T. (2003). The small RNA profile during *Drosophila melanogaster* development. Dev. Cell *5*, 337–350.

Bartel, D.P. (2004). MicroRNAs: Genomics, biogenesis, mechanism, and function. Cell *116*, 281–297.

Bartel, D.P., and Chen, C.Z. (2004). Micromanagers of gene expression: the potentially widespread influence of metazoan microRNAs. Nat. Rev. Genet. *5*, 396–400.

Bergmann, A., Tugentman, M., Shilo, B.Z., and Steller, H. (2002). Regulation of cell number by MAPK-dependent control of apoptosis: A mechanism for trophic survival signaling. Dev. Cell *2*, 159–170.

Boutla, A., Delidakis, C., and Tabler, M. (2003). Developmental defects by antisense-mediated inactivation of micro-RNAs 2 and 13 in Drosophila and the identification of putative target genes. Nucleic Acids Res. *31*, 4973–4980.

Brand, A.H., and Perrimon, N. (1993). Targeted gene expression as a means of altering cell fates and generating dominant phenotypes. Development *118*, 401–415.

Brennecke, J., Hipfner, D.R., Stark, A., Russell, R.B., and Cohen, S.M. (2003). *bantam* encodes a developmentally regulated microRNA that controls cell proliferation and regulates the proapoptotic gene *hid* in *Drosophila*. Cell *113*, 25–36.

Carrington, J.C., and Ambros, V. (2003). Role of microRNAs in plant and animal development. Science *301*, 336–338.

Carroll, S.B. (1990). Zebra patterns in fly embryos: Activation of stripes or repression of interstripes? Cell *60*, 9–16.

Chang, S., Johnston, R.J., Jr., Frokjaer-Jensen, C., Lockery, S., and Hobert, O. (2004). MicroRNAs act sequentially and asymmetrically to control chemosensory laterality in the nematode. Nature *430*, 785–789.

Chen, X. (2004). A microRNA as a translational repressor of APETALA2 in Arabidopsis flower development. Science *303*, 2022–2025.

Chen, P., Nordstrom, W., Gish, B., and Abrams, J.M. (1996). grim, a novel cell death gene in Drosophila. Genes Dev. *10*, 1773–1782.

Christich, A., Kauppila, S., Chen, P., Sogame, N., Ho, S.I., and Abrams, J.M. (2002). The damage-responsive *Drosophila* gene *sickle* encodes a novel IAP binding protein similar to but distinct from *reaper*, *grim*, and *hid*. Curr. Biol. *12*, 137–140.

Doench, J.G., and Sharp, P.A. (2004). Specificity of microRNA target selection in translational repression. Genes Dev. *18*, 504–511.

Enright, A.J., John, B., Gaul, U., Tuschl, T., Sander, C., and Marks, D.S. (2003). MicroRNA targets in Drosophila. Genome Biol. *5*, R1.

Grether, M.E., Abrams, J.M., Agapite, J., White, K., and Steller, H. (1995). The head involution defective gene of Drosophila melanogaster functions in programmed cell death. Genes Dev. *9*, 1694–1708.

Griffiths-Jones, S., Bateman, A., Marshall, M., Khanna, A., and Eddy, S.R. (2003). Rfam: an RNA family database. Nucleic Acids Res. *31*, 439–441.

Hay, B.A. (2000). Understanding IAP function and regulation: a view from Drosophila. Cell Death Differ. *7*, 1045–1056.

Hipfner, D.R., Weigmann, K., and Cohen, S.M. (2002). The bantam gene regulates Drosophila growth. Genetics *161*, 1527–1537.

Hou, X.S., Melnick, M.B., and Perrimon, N. (1996). Marelle acts downstream of the *Drosophila* HOP/JAK kinase and encodes a protein similar to the mammalian STATs. Cell *84*, 411–419.

Hutvágner, G., Simard, M.J., Mello, C.C., and Zamore, P.D. (2004). Sequence-specific inhibition of small RNA function. PLoS Biol. *2*, e98. 10.1371/journal.pbio.0020098.

Jacinto, A., Woolner, S., and Martin, P. (2002). Dynamic analysis of dorsal closure in *Drosophila*: From genetics to cell biology. Dev. Cell *3*, 9–19.

Johnston, R.J., and Hobert, O. (2003). A microRNA controlling left/right neuronal asymmetry in *Caenorhabditis elegans*. Nature *426*, 845–849.

Kennerdell, J.R., and Carthew, R.W. (1998). Use of dsRNA-mediated genetic interference to demonstrate that *frizzled* and *frizzled 2* act in the wingless pathway. Cell *95*, 1017–1026.

Ketting, R.F., and Plasterk, R.H. (2004). What's new about RNAi? Meeting on siRNAs and miRNAs. EMBO Rep. *5*, 762–765.

Lai, E.C. (2004). Predicting and validating miRNA targets. Genome Biol. *5*, 115.

Lai, E.C., Tomancak, P., Williams, R.W., and Rubin, G.M. (2003). Computational identification of Drosophila microRNA genes. Genome Biol. *4*, R42.

Lecuit, T., and Wieschaus, E. (2002). Junctions as organizing centers in epithelial cells? A fly perspective. Traffic *3*, 92–97.

Lee, R.C., Feinbaum, R.L., and Ambros, V. (1993). The *C. elegans* heterochronic gene *lin-4* encodes small RNAs with antisense complementarity to *lin-14*. Cell *75*, 843–854.

Lin, S.Y., Johnson, S.M., Abraham, M., Vella, M.C., Pasquinelli, A., Gamberi, C., Gottlieb, E., and Slack, F.J. (2003). The *C. elegans* hunchback homolog, *hbl-1*, controls temporal patterning and is a probable microRNA target. Dev. Cell *4*, 639–650.

Mazumdar, A., and Mazumdar, M. (2002). How one becomes many: blastoderm cellularization in Drosophila melanogaster. Bioessays *24*, 1012–1022.

Meister, G., Landthaler, M., Dorsett, Y., and Tuschl, T. (2004). Sequence-specific inhibition of microRNA- and siRNA-induced RNA silencing. RNA *10*, 544–550.

Nambu, P.A., and Nambu, J.R. (1996). The Drosophila fish-hook gene encodes a HMG domain protein essential for segmentation and CNS development. Development *122*, 3467–3475.

Nordstrom, W., Chen, P., Steller, H., and Abrams, J.M. (1996). Activation of the reaper gene during ectopic cell killing in Drosophila. Dev. Biol. *180*, 213–226.

Palatnik, J.F., Allen, E., Wu, X., Schommer, C., Schwab, R., Carrington, J.C., and Weigel, D. (2003). Control of leaf morphogenesis by microRNAs. Nature *425*, 257–263.

Pick, L. (1998). Segmentation: painting stripes from flies to vertebrates. Dev. Genet. *23*, 1–10.

Poy, M.N., Eliasson, L., Krutzfeldt, J., Kuwajima, S., Ma, X., Macdonald, P.E., Pfeffer, S., Tuschl, T., Rajewsky, N., Rorsman, P., and Stoffel, M. (2004). A pancreatic islet-specific microRNA regulates insulin secretion. Nature *432*, 226–230.

Rajewsky, N., and Socci, N.D. (2004). Computational identification of microRNA targets. Dev. Biol. *267*, 529–535.

Rehmsmeier, M., Steffen, P., Hochsmann, M., and Giegerich, R. (2004). Fast and effective prediction of microRNA/target duplexes. RNA *10*, 1507–1517.

Reinhart, B.J., Slack, F.J., Basson, M., Pasquinelli, A.E., Bettinger, J.C., Rougvie, A.E., Horvitz, H.R., and Ruvkun, G. (2000). The 21-nucleotide let-7 RNA regulates developmental timing in Caenorhabditis elegans. Nature *403*, 901–906.

Rivera-Pomar, R., and Jackle, H. (1996). From gradients to stripes in Drosophila embryogenesis: filling in the gaps. Trends Genet. *12*, 478–483.

Salvesen, G.S., and Abrams, J.M. (2004). Caspase activation—stepping on the gas or releasing the brakes? Lessons from humans and flies. Oncogene *23*, 2774–2784.

Schock, F., and Perrimon, N. (2002). Molecular mechanisms of epithelial morphogenesis. Annu. Rev. Cell Dev. Biol. *18*, 463–493.

Stark, A., Brennecke, J., Russell, R.B., and Cohen, S.M. (2003). Identification of Drosophila microRNA targets. PLoS Biol. *1*, e60. 10.1371/journal.pbio.0000060.

Tittel, J.N., and Steller, H. (2000). A comparison of programmed cell death between species. Genome Biol. *1*, e60. REVIEWS0003.

Wang, S.L., Hawkins, C.J., Yoo, S.J., Muller, H.A., and Hay, B.A. (1999). The *Drosophila* caspase inhibitor DIAP1 is essential for cell survival and is negatively regulated by HID. Cell *98*, 453–463.

Welte, M.A., Gross, S.P., Postner, M., Block, S.M., and Wieschaus, E.F. (1998). Developmental regulation of vesicle transport in *Drosophila* embryos: Forces and kinetics. Cell *92*, 547–557.

White, K., Grether, M.E., Abrams, J.M., Young, L., Farrell, K., and Steller, H. (1994). Genetic control of programmed cell death in Drosophila. Science *264*, 677–683.

Wightman, B., Ha, I., and Ruvkun, G. (1993). Posttranscriptional regulation of the heterochronic gene *lin-14* by *lin-4* mediates temporal pattern formation in *C. elegans*. Cell *75*, 855–862.

Xu, P., Vernooy, S.Y., Guo, M., and Hay, B.A. (2003). The *Drosophila* microRNA Mir-14 suppresses cell death and is required for normal fat metabolism. Curr. Biol. *13*, 790–795.

Yan, R., Small, S., Desplan, C., Dearolf, C.R., and Darnell, J.E., Jr. (1996). Identification of a *Stat* gene that functions in *Drosophila* development. Cell *84*, 421–430.

Zhang, S., Xu, L., Lee, J., and Xu, T. (2002). *Drosophila* atrophin homolog functions as a transcriptional corepressor in multiple developmental processes. Cell *108*, 45–56.